Engineering Fracture Mechanics 194 (2018) 350–361

Contents lists available at ScienceDirect

Engineering Fracture Mechanics

journal homepage: www.elsevier.com/locate/engfracmech

Effects of nanofiber orientations on the fracture toughness of cellulose nanopaper

Qinghua Meng[a], Bo Li[a], Teng Li[b], Xi-Qiao Feng[a,*]

[a] Institute of Biomechanics and Medical Engineering, AML, Department of Engineering Mechanics, Tsinghua University, Beijing 100084, China
[b] Department of Mechanical Engineering, University of Maryland, College Park, MD 20742, USA

ARTICLE INFO

Keywords:
Cellulose nanopaper
Fracture toughness
Crack-bridging model
Hydrogen bonds

ABSTRACT

Cellulose nanopaper exhibits superior mechanical properties with both high strength and toughness, and the crack bridging mechanism of nanofibers makes the most significant contribution to its fracture toughness. In this paper, we investigate the fracture toughness of a mode-I crack in cellulose nanopaper by using a modified crack-bridging model. Different from previous crack-bridging models, we account for the effect of nanofibers inclined to the crack surfaces. Particular attention is given to the dependence of fracture toughness on the orientation distribution of nanofibers in the cellulose nanopaper. We use a cohesive law to account for the interfacial shear stress of nanofibers, which involve self-healing of hydrogen bonds at their interfaces. Two representative orientation distributions are considered, in which nanofibers are aligned or randomly oriented, respectively. The theoretical results agree well with relevant experiments. This work helps understand the structure–property relationship of cellulose nanopaper and design other fiber-reinforced nanocomposites.

1. Introduction

Cellulose nanofibers, derived from natural materials such as wood and bamboo, have attracted much attention due to their promising applications in bio-based nanomaterials [1–5]. Cellulose nanopaper consisting of a porous network of cellulose nanofibers suggests a bottom-up material design strategy to combine high strength and toughness [6–11]. As yet, however, the mechanical potentials of cellulose nanopaper have not been fully attained because of a lack of understanding of its property–microstructure relation.

Considerable efforts have been dedicated recently toward exploring how to improve the mechanical properties of cellulose nanopaper. For example, nanopaper with a preferred orientation of cellulose nanofibers was fabricated via cold drawing in the wet state [12–14]. The results showed that an increased degree of nanofiber alignment enhances the mechanical stiffness and strength of cellulose nanopaper along the alignment direction. This enhancement effect was also observed in macrofibers made of cellulose nanofibers aligned by wet-stretching [15–18]. Håkansson et al. [19] prepared cellulose filaments by utilizing a surface-charge-controlled gel transition combined with hydrodynamically induced fiber alignment. They showed that those filaments with less aligned fibers exhibit lower stiffness and tensile strength but higher strain at break compared with those made of more aligned fibers. More recently, an anisotropic cellulose nanopaper with highly aligned cellulose nanofibers by delignification and mechanical pressing of natural wood was fabricated by Zhu et al. [20]. They found that the alignment of cellulose nanofibers can dramatically increase the strength and toughness of the resulting anisotropic nanopaper compared with its counterpart without alignment. These

* Corresponding author.
E-mail address: fengxq@tsinghua.edu.cn (X.-Q. Feng).

https://doi.org/10.1016/j.engfracmech.2018.03.034
Received 27 January 2018; Received in revised form 28 March 2018; Accepted 29 March 2018
Available online 03 April 2018
0013-7944/

Nomenclature

δ	crack opening displacement	f	probability density function of nanofiber orientations
θ	orientation angle of a nanofiber	F_b	bridging force
λ	crack-bridging zone length	K_I^0	intrinsic fracture toughness
λ_s	maximal crack-bridging zone length	K_I^∞	stress intensity factor in the far field
σ_∞	tensile stress in the far field	K_I^b	stress intensity factor induced by bridging nanofibers
σ_b	bridging stress	K_I^c	fracture toughness of nanopaper
τ_s	interfacial shear strength between nanofibers	l	average nanofiber length
A	fiber orientation distribution parameter	R	nanofiber radius
E	elastic modulus of nanopaper	V_f	volume fraction of nanofibers

experiments evidenced that nanofiber alignment contributes significantly to the mechanical properties of cellulose nanopaper, and when all nanofibers are aligned along the tensile direction, the full mechanical potentials of cellulose nanopaper can be achieved. To date, however, there has been a lack of theoretical understanding of the nanofiber alignment effects on the mechanical properties of cellulose nanopaper. Fundamental research in this regard would help to design cellulose nanopaper with desirable mechanical performance.

In this paper, therefore, the effect of nanofiber orientations on the fracture toughness of cellulose nanopaper is elucidated by using a modified crack-bridging model. The relation between the fracture toughness and microstructure is established for cellulose nanopaper with either fully aligned or randomly oriented nanofibers.

2. Model and method

2.1. Crack-bridging model

Cellulose nanopaper usually has a porous network microstructure consisting of randomly distributed nanofibers [7–11]. Its mechanical properties can be tuned over a wide range by adjusting the sizes and orientations of nanofibers. In particular, cellulose nanopaper comprising fully aligned nanofibers has anisotropic properties, with the highest strength and toughness along the nanofiber direction [12–14,20]. To examine the effect of nanofiber orientations, therefore, we here compare the fracture toughness of cellulose nanopaper in the following three typical cases of uniaxial tension: (i) all nanofibers are aligned along the tensile direction, (ii) all nanofibers are aligned along a direction deviated from the tensile stress with an angle θ, and (iii) the nanofibers are randomly oriented, as shown in Fig. 1. Other cases of nanofiber orientations can be analyzed analogously.

During loading, the nanofibers embedded in the cellulose nanopaper may slide relatively to each other. As the load increases beyond a threshold, a crack may initiate and propagate. During crack propagation, nanofibers behind the crack tip can be partly

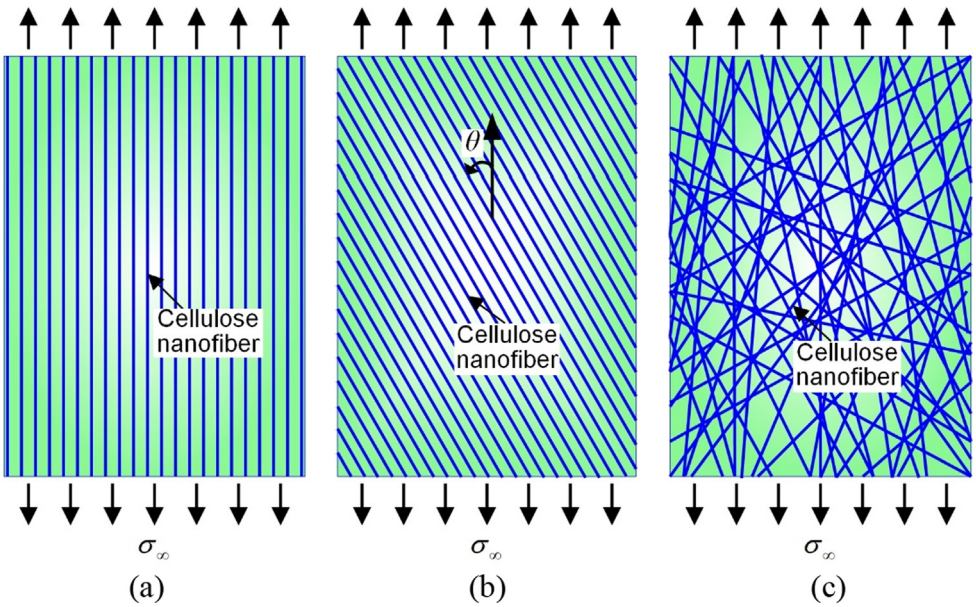

Fig. 1. Schematic of (a) a nanopaper under with fully aligned nanofibers along the tensile stress σ_∞, (b) a nanopaper with fully aligned nanofibers and subjected to tension with an angle θ measured from the fiber direction, and (c) a nanopaper with random nanofibers.

pulled out from one of the two crack surfaces, generating a crack-bridging zone.

In most previous crack-bridging models for fiber-reinforced composites [21–30], the fibers are usually assumed to be perpendicular to the crack surfaces in the crack-bridging zone. In the present work, the classical crack-bridging model is modified to account for the effect of nanofibers inclined to the crack surfaces. For a mode-I crack, the out-pulled segment of each nanofiber in the crack-bridging zone is approximately perpendicular to the crack surfaces. This treatment is reasonable because of the very low bending stiffness of cellulose nanofibers. This method can also be generalized to a mixed-mode crack by assuming that the out-pulled segment of each nanofiber is in alignment with the direction of the crack opening displacement vector.

The relative slipping of nanofibers involves the breakage and reformation of hydrogen bonds at the nanofiber interfaces, which dissipate a large amount of energy and result in a significant enhancement of facture toughness [11,30]. Crack propagation speed may affect the fracture behavior of materials under dynamic conditions [31–33]. In addition, the interfacial sliding behavior may vary with the strain rate, and thus the speed of nanofiber pullout and crack propagation may affect the failure behavior of cellulose nanopaper. In the present paper, however, we ignore this dynamic effect and consider only the case of quasi-static crack propagation. In what follows, we will analyze the contribution of bridging nanofibers and interfacial hydrogen bonds to the fracture toughness of cellulose nanopaper.

We establish a quasi-three-dimensional crack-bridging model of cellulose nanopaper, as shown in Fig. 2a. A semi-infinite model-I crack is subjected to a uniform tensile stress σ_∞ along the y direction in the far field. The nanofibers in the crack-bridging zone

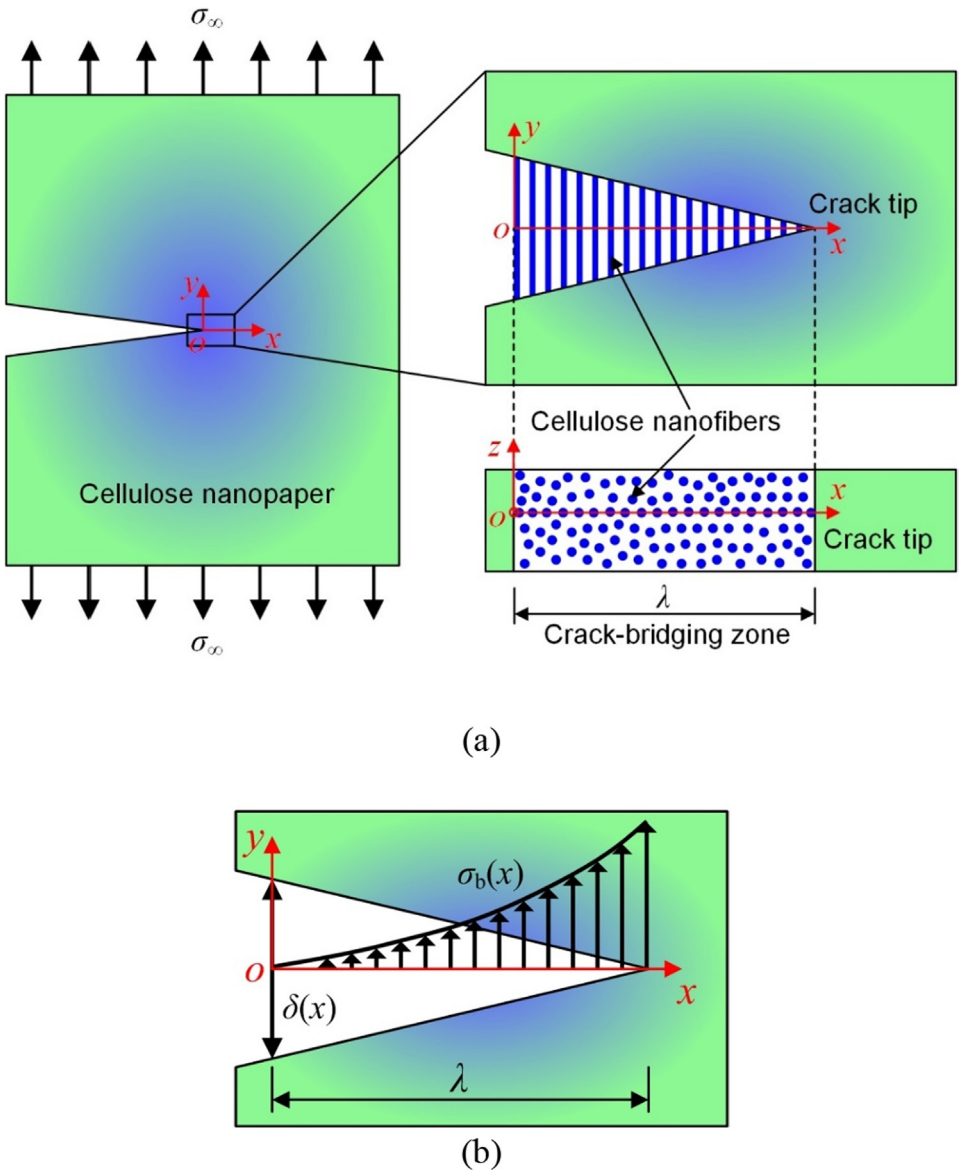

Fig. 2. (a) Crack-bridging model of cellulose nanopaper and (b) schematic of the bridging stress distribution in the crack-bridging zone.

corresponding to the three cases shown in Fig. 1 are schematized in Fig. 3, respectively. To make a direct comparison of their fracture toughnesses, the cellulose nanopaper is treated as an intrinsically homogeneous, isotropic elastic solid with elastic modulus E in all these cases. We use the critical stress intensity factor to evaluate the facture toughness of cellulose nanopaper. For a mode-I crack, the stress intensity factor can be written as [30]

$$K_I^{\infty} = K_I^0 + K_I^b, \tag{1}$$

where K_I^0 denotes the intrinsic fracture toughness of cellulose nanopaper, accounting for energy dissipation induced by intrinsic microscopic damage mechanisms ahead of the crack tip. K_I^{∞} is the stress intensity factor in the far field. When K_I^{∞} reaches a critical value, the crack attains the steady state of propagation, corresponding to a saturated length of the crack-bridging zone and the maximal fracture toughness of cellulose nanopaper, denoted as K_I^c. K_I^b is the stress intensity factor induced by the bridging fibers within the crack-bridging zone. It increases with the crack-bridging zone length and can be calculated by [21]

$$K_I^b = \sqrt{\frac{2}{\pi}} \int_0^{\lambda} \frac{\sigma_b(x)}{\sqrt{\lambda - x}} dx, \tag{2}$$

where λ is the length of the crack-bridging zone, and $\sigma_b(x)$ is the bridging stress at position x in the crack-bridging zone (Fig. 2b). Assume that the bridging nanofibers are discretely distributed in the crack-bridging zone. The discrete bridging forces induced by nanofibers in the crack-bridging zone can be described as a continuous function of cohesive bridging stress $\sigma_b(x)$, which depends on the crack opening displacement $\delta(x)$ in the crack-bridging zone. For a semi-infinite mode-I crack, the crack opening displacement $\delta(x)$ can be expressed as [28,30]

$$\delta(x) = \frac{8K_I^{\infty}\sqrt{\lambda - x}}{\sqrt{2\pi}E} - \frac{4}{\pi E} \int_0^{\lambda} \sigma_b(x) \ln \frac{\sqrt{\lambda - x} + \sqrt{\lambda - \xi}}{|\sqrt{\lambda - x} - \sqrt{\lambda - \xi}|} d\xi, \tag{3}$$

where the first term arises from the far-field stress σ_{∞}, and the second term is caused by the bridging stresses. Since the pullout length of a nanofiber should be no larger than half of its length l, $\delta(x)$ decreases gradually with increasing x and satisfies

$$0 \leqslant \delta(x) \leqslant l/2, \tag{4}$$

where l is the average length of cellulose nanofibers. To calculate the fracture toughness of cellulose nanopaper, the bridging stress $\sigma_b(x)$ and the crack opening displacement $\delta(x)$ should be determined first. Then, $\sigma_b(x)$ and $\delta(x)$ will be solved for the three cases shown in Fig. 1.

2.2. Case 1: Nanopaper under uniaxial tension along the aligned nanofibers

We first consider a cellulose nanopaper consisting of fully aligned nanofibers and subjected to uniaxial tension normal to the mode-I crack, as shown in Fig. 1a. The bridging nanofibers in the crack-bridging zone are shown in Fig. 3a. A cellulose nanofiber that is being pulled out slide with respect to its neighbors, rendering a large interfacial shear stress due to the hydrogen bonds between nanofibers. When the interfacial stress or the sliding displacement reaches a threshold, the hydrogen bonds will be broken but new hydrogen bonds can reform at the interfaces among the relatively sliding nanofibers, as shown in Fig. 4. This self-healing process of hydrogen bonds is repeated until the nanofiber is entirely pulled out. Since cellulose nanofibers primarily interact with each other through hydrogen bonds [7,9,11], the sliding stiffness of their interfaces is weaker than the stiffness of the nanofibers themselves. For

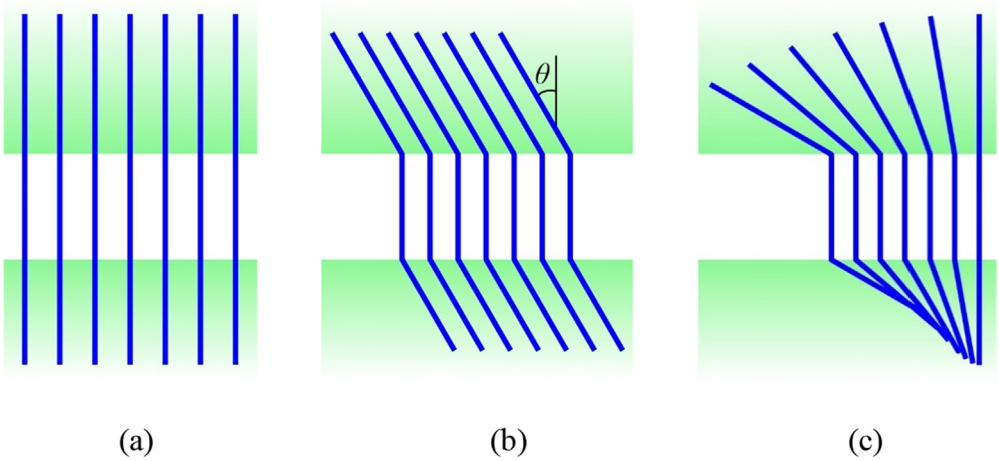

Fig. 3. Bridging nanofibers in the crack-bridging zone of cellulose nanopaper corresponding to the three cases (a)–(c) in Fig. 1. In all cases, the out-pulled segments of nanofibers are assumed to be normal to the crack surfaces (green) because of their very low bending stiffness. (For interpretation of the references to color in this figure legend, the reader is referred to the web version of this article.)

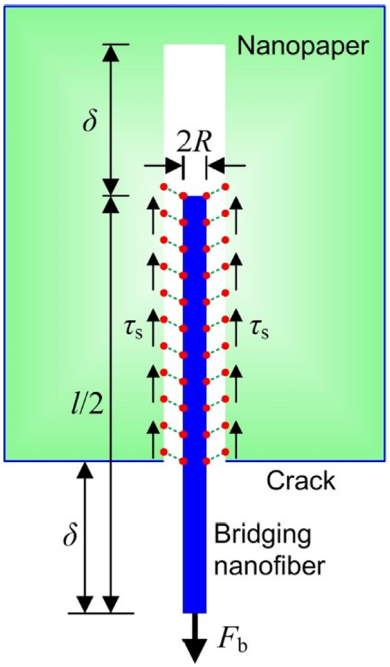

Fig. 4. A nanofiber normal to and partly pulled out from a crack surface.

simplicity, the shear stress is assumed to be uniformly distributed over a relatively sliding interface [30,34,35]. The tensile force F_b on a circular nanofiber and the interfacial shear strength τ_s satisfy the equilibrium condition:

$$F_b = \pi R\tau_s[l-2\delta], \tag{5}$$

where R is the radius of a cellulose nanofiber, and δ is the pullout length of the nanofiber. Since the fibrous structure in a cellulose nanopaper is highly porous [7,11], we adopt V_f to denote the volume fraction of nanofibers in the composite. In the crack-bridging zone, the pullout length of a nanofiber $\delta(x)$ equals the corresponding crack opening displacement at position x. Then according to Eq. (5), the bridging stress $\sigma_b(x)$ at position x is

$$\sigma_b(x) = \frac{V_f\tau_s[l-2\delta(x)]}{R}. \tag{6}$$

Using Eqs. (1), (2), and (6), the stress intensity factor K_I^∞ can be expressed as

$$K_I^\infty = K_I^0 + 2\sqrt{\frac{2}{\pi}}\frac{V_f\tau_s}{R}\left[\sqrt{\lambda}l - \int_0^\lambda \frac{\delta(x)}{\sqrt{\lambda-x}}dx\right]. \tag{7}$$

Substituting Eq. (6) into (3), the crack opening displacement $\delta(x)$ in the crack-bridging zone can be derived as

$$\delta(x) = \frac{8K_I^0\sqrt{\lambda-x}}{\sqrt{2\pi}E} + \frac{4V_f\tau_s l}{\pi ER}\left[2\sqrt{\lambda(\lambda-x)} - x\ln\frac{\sqrt{\lambda}+\sqrt{\lambda-x}}{\sqrt{\lambda}-\sqrt{\lambda-x}}\right] + \frac{8V_f\tau_s}{\pi ER}\int_0^\lambda \delta(\xi)\left(\ln\frac{\sqrt{\lambda-x}+\sqrt{\lambda-\xi}}{|\sqrt{\lambda-x}-\sqrt{\lambda-\xi}|} - \frac{2\sqrt{\lambda-x}}{\sqrt{\lambda-\xi}}\right)d\xi. \tag{8}$$

Eqs. (7) and (8) express the crack opening displacement $\delta(x)$ and the stress intensity factor K_I^∞ of a mode-I crack in cellulose nanopaper with fully aligned nanofibers (Fig. 1a).

When the crack propagation enters a steady state, one has $\delta(x) = l/2$ and the crack-bridging zone approaches a saturated length λ_s. The corresponding stress intensity factor K_I^c is defined as the fracture toughness of the material. It is given by

$$K_I^c = K_I^0 + 2\sqrt{\frac{2}{\pi}}\frac{V_f\tau_s}{R}\left[\sqrt{\lambda_s}l - \int_0^{\lambda_s} \frac{\delta(x)}{\sqrt{\lambda_s-x}}dx\right]. \tag{9}$$

2.3. Case 2: Nanopaper under uniaxial tension inclined to the aligned nanofibers

Now we extend the above model to calculate the fracture toughness of a mode-I crack in a cellulose nanopaper reinforced with aligned nanofibers and subjected to uniaxial tension with an angle θ inclined to the fiber orientation, as shown in Fig. 3b, where $-\pi/2 < \theta < \pi/2$. In the crack-bridging zone, the nanofibers are partly pulled out from one of the crack surfaces. Though the nanofibers originally have an inclined angle to the tensile direction, their out-pulled segments are approximately normal to the crack

surfaces because of the very low bending stiffness of nanofibers, as shown in Fig. 5.

According to the force equilibrium condition, the fiber bridging force F_b in each fiber satisfies the relation:

$$F_b = \pi R\tau_s(l-2\delta)\cos\theta. \tag{10}$$

Using V_f, the bridging stress at position x in the crack-bridging zone can be written as

$$\sigma_b(x) = \frac{V_f\tau_s[l-2\delta(x)]\cos\theta}{R}. \tag{11}$$

Using Eqs. (1), (2), and (11), the stress intensity factor K_I^∞ can be expressed as

$$K_I^\infty = K_I^0 + 2\sqrt{\frac{2}{\pi}}\frac{V_f\tau_s\cos\theta}{R}\left[\sqrt{\lambda}l - \int_0^\lambda \frac{\delta(x)}{\sqrt{\lambda-x}}dx\right]. \tag{12}$$

Thus, the critical stress intensity factor of the mode-I crack in the cellulose nanopaper with fiber alignment angle θ reads

$$K_I^c = K_I^0 + 2\sqrt{\frac{2}{\pi}}\frac{V_f\tau_s\cos\theta}{R}\left[\sqrt{\lambda_s}l - \int_0^{\lambda_s} \frac{\delta(x)}{\sqrt{\lambda_s-x}}dx\right]. \tag{13}$$

Substituting Eqs. (11) and (12) into Eq. (3), the crack opening displacement in the crack-bridging zone is derived as

$$\delta(x) = \frac{8K_I^0\sqrt{\lambda-x}}{\sqrt{2\pi}E} + \frac{4V_f\tau_s l\cos\theta}{\pi ER}\left[2\sqrt{\lambda(\lambda-x)} - x\ln\frac{\sqrt{\lambda}+\sqrt{\lambda-x}}{\sqrt{\lambda}-\sqrt{\lambda-x}}\right] + \frac{8V_f\tau_s\cos\theta}{\pi ER}\int_0^\lambda \delta(\xi)\left(\ln\frac{\sqrt{\lambda-x}+\sqrt{\lambda-\xi}}{|\sqrt{\lambda-x}-\sqrt{\lambda-\xi}|} - \frac{2\sqrt{\lambda-x}}{\sqrt{\lambda-\xi}}\right)d\xi. \tag{14}$$

Eqs. (11) and (14) give the expressions for the stress intensity factor K_I^∞ and the crack opening displacement $\delta(x)$ of a mode-I crack in the cellulose nanopaper.

2.4. Case 3: Nanopaper reinforced with randomly oriented nanofibers

Then we use the crack-bridging model in Section 2.3 to consider a mode-I crack in a cellulose nanopaper containing randomly distributed nanofibers, as shown in Fig. 1c. The random distribution of nanofibers is expressed by a probability density distribution function in terms of their orientation angles θ. The corresponding crack-bridging model is shown in Fig. 3c. Assume that the nanofiber orientations obey the following probability density function:

$$f(\theta) = \frac{A\exp(-A|\theta|)}{2-2\exp(-\pi A/2)}, (-\pi/2 \leqslant \theta \leqslant \pi/2) \tag{15}$$

where A is a constant. The function $f(\theta)$ should satisfy the normalization relation:

$$\int_{-\pi/2}^{\pi/2} f(\theta)d\theta = 1. \tag{16}$$

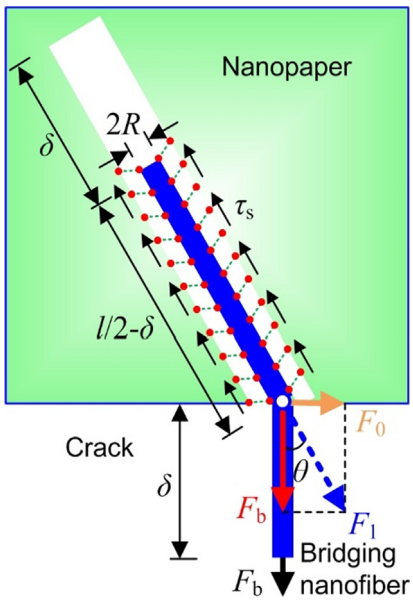

Fig. 5. An originally inclined nanofiber partly pulled out from the crack surface.

According to Eq. (10), the bridging stress $\sigma_b(x)$ at position x in the crack-bridging zone is given as

$$\sigma_b(x) = \frac{V_f \tau_s [l - 2\delta(x)]}{R} \int_{-\pi/2}^{\pi/2} f(\theta) \cos\theta \, d\theta. \tag{17}$$

By integration, Eq. (17) becomes

$$\sigma_b(x) = \frac{V_f \tau_s [l - 2\delta(x)][A^2 + A\exp(-A\pi/2)]}{R(1 + A^2)[1 - \exp(-A\pi/2)]}. \tag{18}$$

Substituting Eqs. (18) and (2) into Eq. (1), the stress intensity factor K_I^∞ of the mode-I crack is expressed as

$$K_I^\infty = K_I^0 + \frac{2\sqrt{2} V_f \tau_s [A^2 + A\exp(-A\pi/2)]}{\sqrt{\pi} R(1 + A^2)[1 - \exp(-A\pi/2)]} \left[\sqrt{\lambda} l - \int_0^\lambda \frac{\delta(x)}{\sqrt{\lambda - x}} dx \right]. \tag{19}$$

Then substituting Eqs. (18) and (19) into Eq. (3), the crack opening displacement $\delta(x)$ in the crack-bridging zone can be derived as

$$\delta(x) = \frac{8K_I^0 \sqrt{\lambda - x}}{\sqrt{2\pi} E} + \frac{8V_f \tau_s [A^2 + A\exp(-A\pi/2)]}{\pi E R(1 + A^2)[1 - \exp(-A\pi/2)]} \left[\sqrt{\lambda(\lambda - x)} l - \frac{xl}{2} \ln \frac{\sqrt{\lambda} + \sqrt{\lambda - x}}{\sqrt{\lambda} - \sqrt{\lambda - x}} + \int_0^\lambda \delta(\xi) \left(\ln \frac{\sqrt{\lambda - x} + \sqrt{\lambda - \xi}}{|\sqrt{\lambda - x} - \sqrt{\lambda - \xi}|} - \frac{2\sqrt{\lambda - x}}{\sqrt{\lambda - \xi}} \right) d\xi \right]. \tag{20}$$

Eqs. (19) and (20) provide the stress intensity factor K_I^∞ and the crack opening displacement $\delta(x)$ for a mode-I crack in cellulose nanopaper with randomly oriented nanofibers. When the crack enters a steady state of propagation, the corresponding critical stress intensity factor K_I^c will be regarded as the fracture toughness of the material. It is obtained as

$$K_I^c = K_I^0 + \frac{2\sqrt{2} V_f \tau_s [A^2 + A\exp(-A\pi/2)]}{\sqrt{\pi} R(1 + A^2)[1 - \exp(-A\pi/2)]} \left[\sqrt{\lambda_s} l - \int_0^{\lambda_s} \frac{\delta(x)}{\sqrt{\lambda_s - x}} dx \right]. \tag{21}$$

2.5. Unified expression

In Sections 2.2–2.4, the stress intensity factor K_I^∞ and the crack opening displacement $\delta(x)$ of a mode-I crack have been given for three typical cases of nanofiber orientations, which can be expressed as a unified form. For example, Eqs. (7), (12), and (19) can be unified as

$$K_{I\alpha}^\infty = K_I^0 + 2\sqrt{\frac{2}{\pi}} \frac{V_f \tau_s c_\alpha}{R} \left[\sqrt{\lambda} l - \int_0^\lambda \frac{\delta(x)}{\sqrt{\lambda - x}} dx \right], \tag{22}$$

where $c_1 = 1$, $c_2 = \cos\theta$, and $c_3 = \frac{A^2 + A\exp(-A\pi/2)}{(1 + A^2)[1 - \exp(-A\pi/2)]}$, with $\alpha = 1, 2, 3$ standing for the three cases (a)–(c) in Fig. 1, respectively. Correspondingly, the critical stress intensity factors in Eqs. (9), (13), and (21) are re-expressed as

$$K_{I\alpha}^c = K_I^0 + 2\sqrt{\frac{2}{\pi}} \frac{V_f \tau_s c_\alpha}{R} \left[\sqrt{\lambda_s} l - \int_0^{\lambda_s} \frac{\delta(x)}{\sqrt{\lambda_s - x}} dx \right]. \tag{23}$$

The crack opening displacements in the crack-bridging zone in Eqs. (8), (14), and (20) can be unified as

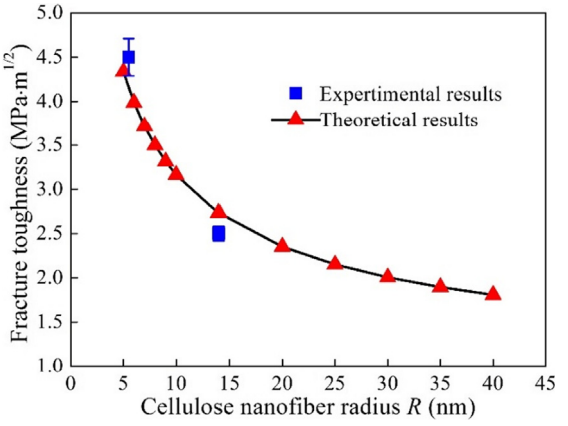

Fig. 6. Fracture toughness of cellulose nanopaper with randomly oriented nanofibers as a function of the radius of constituent nanofibers.

$$\delta_\alpha(x) = \frac{8K_I^0\sqrt{\lambda-x}}{\sqrt{2\pi}E} + \frac{4V_f\tau_s l c_\alpha}{\pi ER}\left[2\sqrt{\lambda(\lambda-x)} - x\ln\frac{\sqrt{\lambda}+\sqrt{\lambda-x}}{\sqrt{\lambda}-\sqrt{\lambda-x}}\right] + \frac{8V_f\tau_s c_\alpha}{\pi ER}\int_0^\lambda \delta(\xi)\left(\ln\frac{\sqrt{\lambda-x}+\sqrt{\lambda-\xi}}{|\sqrt{\lambda-x}-\sqrt{\lambda-\xi}|} - \frac{2\sqrt{\lambda-x}}{\sqrt{\lambda-\xi}}\right)d\xi. \tag{24}$$

Because the equations for the bridging stress $\sigma_b(x)$ and the crack opening displacement $\delta(x)$ in the crack-bridging zone are coupled, it is hard to solve them analytically. Therefore, a numerical iteration method is invoked to solve K_I^∞ and $\delta(x)$ from Eqs. (22) and (24), as described in Appendix A.

3. Results and discussion

3.1. Fracture toughness of nanopaper with randomly oriented nanofibers

We first use the crack-bridging model to predict the fracture toughness of cellulose nanopaper with randomly oriented nanofibers, as shown in Fig. 6. The material parameters used in our calculations are listed in Table 1, except stated elsewhere. The nanofibers in cellulose paper normally have a radius in the range from several to tens nanometers. When we take the nanofiber radius R as 5.5 nm and 14 nm, the theoretical fracture toughnesses of nanopaper are obtained as 4.3 MPa·m$^{1/2}$ and 2.7 MPa·m$^{1/2}$, respectively. The corresponding experimental values are about 4.5 MPa·m$^{1/2}$ and 2.5 MPa·m$^{1/2}$ [11,30], demonstrating a good agreement between our theoretical predictions and the experimental data. By calibrating the theoretical fracture toughness to the experiment results of Zhu et al. [11], we determine the fiber orientation distribution parameter $A = -1$. This is reasonable since $A = -1$ corresponds to an isotropic nanopaper with fully randomly oriented nanofibers.

Fig. 6 also shows that the fracture toughness of nanopaper is highly sensitive to the characteristic sizes of its constituent cellulose nanofibers. For a specified nanofiber length, the fracture toughness of nanopaper increases with the decrease in the radius of the fibers. Under a fixed volume fraction of nanofibers, reducing nanofiber radius will increase the overall interfacial area and the number of hydrogen bonds, thereby yielding a significant enhancement in the fracture toughness of nanopaper. The rich hydroxyl groups along the cellulose molecular chains allow for facile formation and reformation of hydrogen bonds at the nanofiber interfaces, enhancing the macroscopic fracture toughness of nanopaper [11].

3.2. Effects of nanofiber orientation distribution

In this subsection, we examine the effects of nanofiber orientation distribution on the fracture toughness of cellulose nanopaper. The nanofiber orientation distribution is expressed by, for instance, the probability density function $f(\theta)$ in Eq. (15), with the fiber orientation angle in the range of $-\pi/2 \leqslant \theta \leqslant \pi/2$. For different values of the parameter A, Fig. 7 shows the probability density function $f(\theta)$. It can be seen that for a small positive value of A (e.g., 0.1), the nanofibers are uniformly distributed in the range of orientations from $-\pi/2$ to $\pi/2$. For a large positive value of A (e.g., 10.0), almost all nanofibers are aligned along the direction of $\theta = 0°$ or, in other words, normal to the crack surfaces. For a large negative value of A (e.g., –10.0), most nanofibers are along the direction of $\theta = \pm\pi/2$ and normal to the tensile direction. These results suggest that the proposed probability distribution function can reasonably describe the random distribution of cellulose nanofibers.

For different nanofiber orientation distributions $f(\theta)$, Fig. 8 shows the variation in the fracture toughness of cellulose nanopaper with respect to A. Evidently, the fracture toughness of nanopaper increases with increasing A. As A is sufficiently large (e.g., $A = 100$), the fracture toughness approaches the constant $K_I^c = 3.7$ MPa·m$^{1/2}$, which is the fracture toughness of a mode-I crack in a nanopaper where all nanofibers are normal to the crack. When A is very small (e.g., $A = -100$), the fracture toughness approaches another constant, $K_I^c = 1.0$ MPa·m$^{1/2}$, which is the intrinsic fracture toughness without accounting for the crack-bridging mechanism or, in other words, the fracture toughness of a nanopaper where all nanofibers are parallel to the crack ($\theta = \pm\pi/2$).

The above results demonstrate a significant influence of nanofiber orientation distribution on the fracture toughness of nanopaper, as observed in experiments [12,14,20]. When all fibers are oriented along the tensile direction, the fracture toughness of nanopaper reaches its maximum value. Such highly anisotropic nanopaper can be further made into strands with superior strength and toughness.

Table 1
Material parameters used in our calculations.

Parameters	Value	References
Elastic modulus E	13.5 GPa	Sehaqui et al. [8]
Fracture toughness K_I^0	1.0 MPa·m$^{1/2}$	Meng et al. [30]
Interfacial shear strength τ_s	30.0 MPa	Meng et al. [30]
Nanofiber radius R	14.0 nm	Zhu et al. [11]
Nanofiber length l	1.5 μm	Moon et al. [2]
Nanofiber volume fraction V_f	80%	–
Distribution parameter A	−1	–

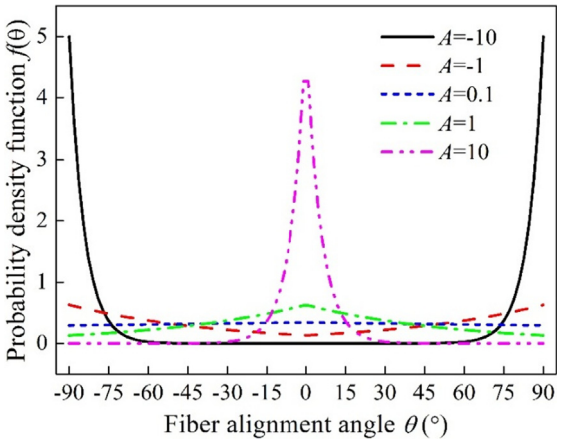

Fig. 7. Orientation distribution functions of nanofibers for different values of parameter *A*.

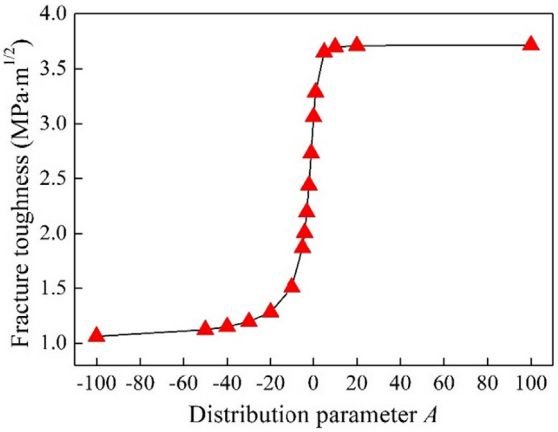

Fig. 8. Variation in the fracture toughness of nanopaper with respect to the nanofiber orientation distribution parameter *A*.

3.3. Fracture toughness of nanopaper with aligned nanofibers

Now we consider the fracture toughness of a mode-I crack in a nanopaper with fully aligned nanofibers. To examine the directional dependence of fracture toughness, the normal direction of the crack is assumed to have an inclined angle θ from the nanofiber orientation, as shown in Fig. 3b. Without loss of generality, we take $0 \leqslant \theta \leqslant \pi/2$. Fig. 9a shows the crack opening displacement in the crack-bridging zone of a steadily propagating crack under different values of θ. The crack opening displacement approaches zero at the crack tip. A smaller alignment angle gives rise to a smaller crack opening displacement, indicative of that a smaller alignment angle tends to hinder the crack propagation of nanopaper. For a steadily propagating crack, Fig. 9b and c show the bridging zone length and the fracture toughness of nanopaper with respect to the fiber alignment angle, respectively. The bridging zone length exponentially increases as the fiber alignment angle increases, demonstrating that smaller alignment angles enable a stronger toughening effect. With decreasing fiber alignment angle, the fracture toughness of nanopaper exponentially increases, suggesting that the nanopaper with fully aligned nanofibers can exhibit superior mechanical properties by choosing loading direction. As the fiber alignment angle decreases, the alignment fibers support a higher load along the loading direction and the hydrogen bonds at the interfaces dissipate more energy, improving the fracture toughness of anisotropic nanopaper. These results reveal that the mechanical properties of such an anisotropic nanopaper can be given to full play by adjusting the fiber alignment direction, thus providing a theoretical guidance for designing advanced nanopaper.

4. Conclusions

A theoretical model has been developed to evaluate the effect of nanofiber alignment in the fracture toughness of cellulose nanopaper. A probability density function with an exponential form is proposed to describe the random distribution of nanofibers in nanopaper. It is found that the fracture toughness of nanopaper strongly depends on the alignment degree of nanofibers. The fracture toughness of nanopaper with aligned nanofibers along the loading direction can be much higher than that of nanopaper with randomly distributed nanofibers. An increased alignment degree of nanofibers tends to improve the mechanical properties of nanopaper.

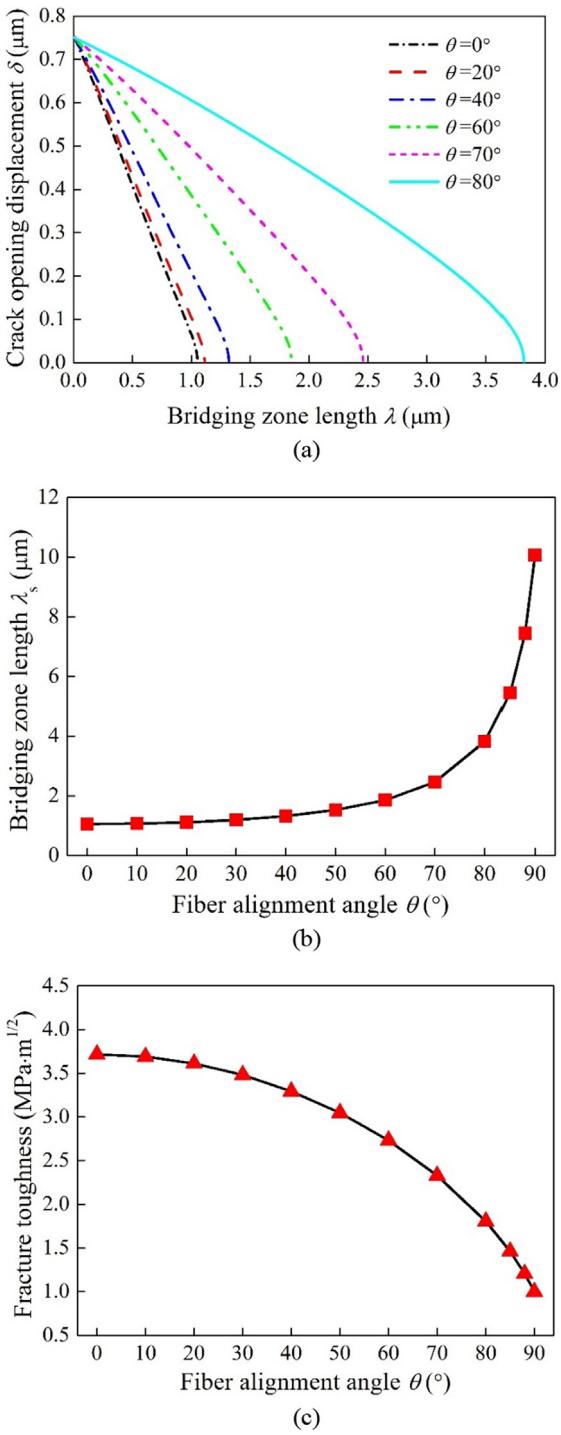

Fig. 9. (a) Crack opening displacement in the crack-bridging zone of a steady propagation crack under different fiber alignment angles. (b) The bridging zone length and (c) the fracture toughness of cellulose nanopaper with respect to the fiber alignment angle.

The nanopaper with fully aligned nanofibers can achieve the highest mechanical properties in the fiber alignment direction. The theoretical prediction for the fracture toughness of nanopaper agrees well with the experimental results. The present crack-bridging model can also be used to analyze composites reinforced by carbon nanotubes and other nanofibers [36,37]. This work offers a theoretical basis for engineering and optimizing advanced cellulose functional materials.

Acknowledgments

This work was supported by the National Natural Science Foundation of China (Grant Nos. 11432008 and 11672161), China Postdoctoral Science Foundation (Grant No. 2016M590092), and the Thousand Young Talents Program of China are acknowledged. TL acknowledges the support from the NIA Distinguished Langley Professor Program.

Appendix A

The stress intensity factor K_I^{∞} and the crack opening displacement $\delta(x)$ for the crack in cellulose nanopaper are obtained by solving Eqs. (22) and (24) in the main text via a numerical method including the following five main steps:

Step 1: Set a small value for the initial length of the bridging zone length, λ_0. Then, we increase the value of λ gradually in the iteration process to simulate the extension of the crack-bridging zone with loading. For each λ, the crack-bridging zone $(0 \leqslant x \leqslant \lambda)$ is divided into $N = \lambda/\Delta x$ subintervals, with the sequentially numbered points $0 < x_1 < \cdots < x_i < \cdots < x_N < \lambda$, where $x_i = (i-1/2)\Delta x$ and Δx is the length of each subinterval. The crack opening displacements at these points are denoted by $\delta_\alpha(x_i)$, with $i = 1,2,...,N$.

Step 2: Using Eq. (24) in main text, the crack opening displacement $\delta_\alpha(x_i)$ at position x_i can be given by

$$\delta_\alpha(x_i) = \frac{8K_I^0\sqrt{\lambda-x_i}}{\sqrt{2\pi}E} + \frac{4V_f\tau_s l c_\alpha}{\pi ER}\left(2\sqrt{\lambda(\lambda-x_i)} - x_i \ln\frac{\sqrt{\lambda}+\sqrt{\lambda-x_i}}{\sqrt{\lambda}-\sqrt{\lambda-x_i}}\right) + \frac{8V_f\tau_s\Delta x c_\alpha}{\pi ER}\sum_{\substack{j=1\\ j\neq i}}^{N}\delta(x_j)\left(\ln\frac{\sqrt{\lambda-x_i}+\sqrt{\lambda-x_j}}{|\sqrt{\lambda-x_i}-\sqrt{\lambda-x_j}|} - \frac{2\sqrt{\lambda-x_i}}{\sqrt{\lambda-x_j}}\right)$$
$$+\frac{8V_f\tau_s\Delta x\delta(x_i)c_\alpha}{\pi ER}\left(\ln\frac{\sqrt{\lambda-x_i}+\sqrt{\lambda-x_i-\xi}}{\sqrt{\lambda-x_i}-\sqrt{\lambda-x_i-\xi}} - 2\right), \tag{A1}$$

where ξ is a small positive constant. In the calculations, we set $\xi = 10^{-11}$.

Step 3: From the crack opening displacement in Eq. (A1) at each position x_i, we obtain a system of linear equations with unknowns $\delta_\alpha(x_i)$. We numerically solve them to determine the crack opening displacement distribution over the entire crack-bridging zone.

Step 4: Using the crack opening displacement function $\delta_\alpha(x_i)$ obtained in Step 3, we calculate the stress intensity factor K_I^{∞} by

$$K_{I\alpha}^{\infty} = K_I^0 + 2\sqrt{\frac{2}{\pi}}\frac{V_f\tau_s c_\alpha}{R}\left[\sqrt{\lambda}\, l - \sum_{i=1}^{N}\frac{\Delta x\delta(x_i)}{\sqrt{\lambda-x_i}}\right]. \tag{A2}$$

Step 5: When the maximal crack opening displacement $\delta_\alpha(x_N)$ in the crack-bridging zone reaches half of the average fiber length, $l/2$, the nanofiber will be fully pulled out, indicating that the bridging zone has reached the maximal or saturated length and the crack has entered a steady state of propagation. Then we stop the iteration, and determine the maximal crack-bridging zone length λ_s and the fracture toughness $K_{I\alpha}^c$ of the material from this state.

References

[1] Klemm D, Kramer F, Moritz S, Lindström T, Ankerfors M, Gray D, et al. Nanocelluloses: A new family of nature-based materials. Angew Chem-Int Ed 2011;50(24):5438–66.
[2] Moon RJ, Martini A, Nairn J, Simonsen J, Youngblood J. Cellulose nanomaterials review: structure, properties and nanocomposites. Chem Soc Rev 2011;40(7):3941–94.
[3] Lee KY, Aitomäki Y, Berglund LA, Oksman K, Bismarck A. On the use of nanocellulose as reinforcement in polymer matrix composites. Compos Sci Technol 2014;105:15–27.
[4] Jiang F, Li T, Li Y, Zhang Y, Gong A, Dai J, et al. Wood-based nanotechnologies toward sustainability. Adv Mater 2018;30(1):1703453.
[5] Song J, Chen C, Zhu S, Zhu M, Dai J, Ray U, et al. Processing bulk natural wood into a high-performance structural material. Nature 2018;554:224–8.
[6] Benítez AJ, Walther A. Cellulose nanofibril nanopapers and bioinspired nanocomposites: a review to understand the mechanical property space. J Mater Chem A 2017;5:16003–24.
[7] Henriksson M, Berglund LA, Isaksson P, Lindstrom T, Nishino T. Cellulose nanopaper structures of high toughness. Biomacromolecules 2008;9(6):1579–85.
[8] Sehaqui H, Zhou Q, Ikkala O, Berglund LA. Strong and tough cellulose nanopaper with high specific surface area and porosity. Biomacromolecules 2011;12(10):3638–44.
[9] Sehaqui H, Allais M, Zhou Q, Berglund LA. Wood cellulose biocomposites with fibrous structures at micro-and nanoscale. Compos Sci Technol 2011;71(3):382–7.
[10] Salajkova M, Valentini L, Zhou Q, Berglund LA. Tough nanopaper structures based on cellulose nanofibers and carbon nanotubes. Compos Sci Technol 2013;87:103–10.
[11] Zhu H, Zhu S, Jia Z, Parvinian S, Li Y, Vaaland O, et al. Anomalous scaling law of strength and toughness of cellulose nanopaper. Proc Natl Acad Sci U S A 2015;112(29):8971–6.
[12] Sehaqui H, Ezekiel Mushi N, Morimune S, Salajkova M, Nishino T, Berglund LA. Cellulose nanofiber orientation in nanopaper and nanocomposites by cold drawing. ACS Appl Mater Interfaces 2012;4(2):1043–9.
[13] Sehaqui H, Morimune S, Nishino T, Berglund LA. Stretchable and strong cellulose nanopaper structures based on polymer-coated nanofiber networks: An alternative to nonwoven porous membranes from electrospinning. Biomacromolecules 2012;13(11):3661–7.
[14] Wang S, Li T, Chen C, Kong W, Zhu S, Dai J, et al. Transparent, anisotropic biofilm with aligned bacterial cellulose nanofibers. Adv Funct Mater 2018:1707491. http://dx.doi.org/10.1002/adfm.201707491.

[15] Iwamoto S, Isogai A, Iwata T. Structure and mechanical properties of wet-spun fibers made from natural cellulose nanofibers. Biomacromolecules 2011;12(3):831–6.
[16] Walther A, Timonen JV, Díez I, Laukkanen A, Ikkala O. Multifunctional high-performance biofibers based on wet-extrusion of renewable native cellulose nanofibrils. Adv Mater 2011;23(26):2924–8.
[17] Torres-Rendon JG, Schacher FH, Ifuku S, Walther A. Mechanical performance of macrofibers of cellulose and chitin nanofibrils aligned by wet-stretching: a critical comparison. Biomacromolecules 2014;15(7):2709–17.
[18] Wang S, Jiang F, Xu X, Kuang Y, Fu K, Hitz E, et al. Super-strong, super-stiff macrofibers with aligned, long bacterial cellulose nanofibers. Adv Mater 2017;29(35):1702498.
[19] Håkansson KMO, Fall AB, Lundell F, Yu S, Krywka C, Roth SV, et al. Hydrodynamic alignment and assembly of nanofibrils resulting in strong cellulose filaments. Nat Commun 2014;5:4018.
[20] Zhu M, Wang Y, Zhu S, Xu L, Jia C, Dai J, et al. Anisotropic, transparent films with aligned cellulose nanofibers. Adv Mater 2017;29(21):1606284.
[21] Budiansky B, Amazigo JC. Toughening by aligned, frictionally constrained fibers. J Mech Phys Solids 1989;37(1):93–109.
[22] Rubinstein AA, Xu K. Micromechanical model of crack growth in fiber-reinforced ceramics. J Mech Phys Solids 1992;40(1):105–25.
[23] Bao G, Song Y. Crack bridging models for fiber composites with slip-dependent interfaces. J Mech Phys Solids 1993;41(9):1425–44.
[24] Meda G, Steif PS. A detailed analysis of cracks bridged by fibers-I. Limiting cases of short and long cracks. J Mech Phys Solids 1994;42(8):1293–321.
[25] Budiansky B, Cui YL. Toughening of ceramics by short aligned fibers. Mech Mater 1995;21(2):139–46.
[26] Liu YF, Masuda C, Yuuki R. Effect of microstructural parameters on the fracture behavior of fiber-reinforced ceramics. Mech Mater 1998;29(2):111–21.
[27] Nemat-Nasser S, Ni L. A fiber-bridged crack with rate-dependent bridging forces. J Mech Phys Solids 2001;49(11):2635–50.
[28] Shao Y, Zhao HP, Feng XQ, Gao H. Discontinuous crack-bridging model for fracture toughness analysis of nacre. J Mech Phys Solids 2012;60(8):1400–19.
[29] Shao Y, Zhao HP, Feng XQ. On flaw tolerance of nacre: a theoretical study. J R Soc Interface 2014;11(92):20131016.
[30] Meng QH, Li B, Li T, Feng XQ. A multiscale crack-bridging model of cellulose nanopaper. J Mech Phys Solids 2017;103:22–39.
[31] Buehler MJ, Abraham FF, Gao H. Hyperelasticity governs dynamic fracture at a critical length scale. Nature 2003;426(6963):141–6.
[32] Buehler MJ, Gao H. Dynamical fracture instabilities due to local hyperelasticity at crack tips. Nature 2006;439(7074):307–10.
[33] Kermode JR, Albaret T, Sherman D, Bernstein N, Gumbsch P, Payne MC, et al. Low-speed fracture instabilities in a brittle crystal. Nature 2008;455(7217):1224–7.
[34] Ji B, Gao H. Mechanical properties of nanostructure of biological materials. J Mech Phys Solids 2004;52(9):1963–90.
[35] Liu G, Ji B, Hwang KC, Khoo BC. Analytical solutions of the displacement and stress fields of the nanocomposite structure of biological materials. Compos Sci Technol 2011;71(9):1190–5.
[36] Fu SY, Feng XQ, Lauke B, Mai YW. Effects of particle size, particle/matrix interface adhesion and particle loading on mechanical properties of particulate-polymer composites. Compos Part B-Eng 2008;39(6):933–61.
[37] Shi DL, Feng XQ, Huang Y, Hwang KC, Gao H. The effect of nanotube waviness and agglomeration on the elastic property of carbon nanotube-reinforced composites. J Eng Mater Technol-Trans ASME 2004;126(3):250–7.